University of Groningen

Radio interferometric calibration using the SAGE algorithm

Kazemi, S.; Yatawatta, S.; Zaroubi, S.; Lampropoulos, P.; de Bruyn, A. G.; Koopmans, L. V. E.; Noordam, J.

IMPORTANT NOTE: You are advised to consult the publisher's version (publisher's PDF) if you wish to cite from it. Please check the document version below.

Document Version
Publisher's PDF, also known as Version of record

Link to publication in University of Groningen/UMCG research database

Radio interferometric calibration using the SAGE algorithm

S. Kazemi,[1]★ S. Yatawatta,[1,2] S. Zaroubi,[1,3] P. Lampropoulos,[1,2] A. G. de Bruyn,[1,2] L. V. E. Koopmans[1] and J. Noordam[2]

[1]*Kapteyn Astronomical Institute, University of Groningen, PO Box 800, 9700 AV Groningen, the Netherlands*
[2]*ASTRON, Postbus 2, 7990 AA Dwingeloo, the Netherlands*
[3]*Physics Department, Technion, Haifa 32000, Israel*

ABSTRACT

The aim of the new generation of radio synthesis arrays such as LOw Frequency ARray (LOFAR) and Square Kilometre Array (SKA) is to achieve much higher sensitivity, resolution and frequency coverage than what is available now, especially at low frequencies. To accomplish this goal, the accuracy of the calibration techniques used is of considerable importance. Moreover, since these telescopes produce huge amounts of data, speed of convergence of calibration is a major bottleneck. The errors in calibration are due to system noise (sky and instrumental) as well as the estimation errors introduced by the calibration technique itself, which we call 'solver noise'. We define solver noise as the 'distance' between the optimal solution (the true value of the unknowns, uncorrupted by the system noise) and the solution obtained by calibration. We present the Space Alternating Generalized Expectation Maximization (SAGE) calibration technique, which is a modification of the Expectation Maximization algorithm, and compare its performance with the traditional least squares calibration based on the level of solver noise introduced by each technique. For this purpose, we develop statistical methods that use the calibrated solutions to estimate the level of solver noise. The SAGE calibration algorithm yields very promising results in terms of both accuracy and speed of convergence. The comparison approaches that we adopt introduce a new framework for assessing the performance of different calibration schemes.

Key words: methods: numerical – methods: statistical – techniques: interferometric.

1 INTRODUCTION

Early radio astronomy predominantly used single dishes for observations. With the resolution requirements increasing, the single-dish approach became impractical. This paved the path for using radio-interferometric techniques with multiple antennas linked together as an array that operates as a large effective single dish (Thompson, Moran & Swenson 2001).

The sensitivity of an interferometer is greatly increased, compared to a single-dish telescope, due to the larger combined collecting area. The currently planned or built radio interferometers, such as the Square Kilometre Array (SKA),[1] the Murchison Widefield Array (MWA),[2] the Precision Array to Probe Epoch of Reionization (PAPER),[3] the 21-cm Array (21CMA),[4] the Hydrogen Epoch of Reionization Array (HERA),[5] the Long Wavelength Array (LWA)[6] and the LOw Frequency ARray (LOFAR),[7] consist of a large number of elements and include short, intermediate and many of them longer antenna spacings. For an introduction to radio interferometry we refer the reader to Thompson et al. (2001).

In the interferometric visibilities, there always exist errors introduced by the sky, the atmosphere (e.g. troposphere and ionosphere), the instrument (e.g. beam-shape, frequency response, receiver gains, etc.) and Radio Frequency Interference (RFI). The process of estimating and reducing the errors in these measurements is called 'calibration' and is an essential step before imaging the visibilities.

The classical calibration method, named external (or primary) calibration, is based on observing a celestial radio source with known properties. This approach is strongly dependent on the accuracy with which the source properties are known. The external calibration is improved by using self-calibration (Pearson &

★E-mail: kazemi@astro.rug.nl
[1] http://www.skatelescope.org
[2] http://www.mwatelescope.org
[3] http://astro.berkeley.edu/~dbacker/eor
[4] http://21cma.bao.ac.cn

[5] http://www.reionization.org
[6] http://lwa.unm.edu
[7] http://www.lofar.org

Readhead 1984) which utilizes the observed data for estimating both the unknown instrumental and the sky parameters. The quality of calibration and the imaging is significantly increased by iterating between the sky and the instrument model. The redundant calibration is also independent of the sky model. It calibrates for both the sky and the instrument, using redundant information in the measured data. However, its performance is limited to arrays with a regular arrangement in their antennas' layout.

Calibration is an optimization process that is non-linear by nature. It is in essence a maximum likelihood (ML) estimation of the unknown parameters by applying non-linear optimization techniques. Traditional calibration is estimating the ML solution by the non-linear least squares (LS) method via various gradient-based techniques such as the Levenberg–Marquardt (LM) algorithm (Levenberg 1944; Marquardt 1963). This approach was improved by the Expectation Maximization (EM) algorithm (Feder & Weinstein 1988) and later on by the Space Alternating Generalized Expectation Maximization (SAGE) technique which was introduced by Fessler & Hero (1994) and was applied to interferometer calibration by Yatawatta et al. (2009). The analysis and application of the aforementioned schemes for the calibration of radio interferometers can be found in Yatawatta et al. (2009).

To reach the scientific goals of the new generation of radio arrays, calibration algorithms must have the highest accuracy possible. Furthermore, the number of measured visibilities that has to be calibrated is unprecedented. The speed of convergence of the calibration processes must therefore be the fastest with the minimum possible computational cost. Based on these facts, the best calibration method is referred to as the one which minimizes the 'distance' between the true values of unknown parameters and the values obtained by calibration and minimizes computational time.

We should take into account that the measured data of an interferometer is always corrupted by different sources of noise such as the thermal noise, which is an additive Gaussian random process, and confusion noise (Condon 1974), which affects the coherency matrix [see the next section and e.g. Born & Wolf (1999)]. For a detailed discussion on the sources of noise the reader is referred to the chapter 6 of Wijnholds (2010). When the calibration process of the measured data is done, the 'distance' between the true value of the unknown parameters and their calibrated solutions depends on the initial noise and the errors originating from the calibration process itself (e.g. converging to a local minimum), which is called 'solver noise'. In other words, because the calibrated solutions are not optimal, there always exists some solver noise between these solutions and the true values of the unknown parameters affected by the initial noise. The lower the solver noise, the higher the accuracy of the calibrated results. Thus, in order to increase the calibration efficiency, we need to choose the calibration scheme which has the minimum solver noise as well as the lowest computational cost. To achieve this, we should be able to compare these two factors between various calibration techniques. We introduce a general framework for detecting the level of solver noise in calibration algorithms based only on their solutions.

In this paper, we present the SAGE calibration method and emphasize its superiority, compared to the traditional LS calibration, in terms of accuracy and speed of convergence. Mathematical derivations of the algorithms are presented in the Appendices. We also investigate the applicability of two well-known measures, the Kullback–Leibler Divergence (KLD) (Kullback 1997) and the likelihood-ratio test (LRT) (Graves 1978) in revealing the level of solver noise in calibrated solutions. Illustrative examples of both real and simulated observations show the superior performance of the SAGE calibration compared to the LS one. They also indicate that the LRT approach is very promising at detecting the level of solver noise in the obtained calibrated solutions, while the KLD approach is not always conclusive.

The following notations are used in this paper: bold, lowercase letters refer to column vectors, e.g. $\boldsymbol{y}$, and upper case bold letters refer to matrices, e.g. $\mathbf{C}$. All parameters are complex numbers, unless stated otherwise. The inverse, transpose, Hermitian transpose and conjugation of a matrix are presented by $(\cdot)^{-1}$, $(\cdot)^{\mathrm{T}}$, $(\cdot)^{\mathrm{H}}$ and $(\cdot)*$, respectively. The statistical expectation operator is referred to as $E\{\cdot\}$. The matrix Kronecker product and the proper (strict) subset are denoted by $\otimes$ and $\subsetneq$, respectively. The diagonal matrix consisting of only the diagonal entries of a square matrix is given by $\mathrm{diag}(\cdot)$. $\mathbf{I}$ is the identity matrix and $\varnothing$ is the empty set. The Kronecker delta function is presented by δ_{ij}. $\mathbb{R}$ and $\mathbb{C}$ are the sets of Real and Complex numbers, respectively. The Frobenius norm is shown by $||\cdot||$. Estimated parameters are denoted by a hat, $\widehat{(\cdot)}$. All logarithmic calculations are to the base e.

2 THE MEASUREMENT EQUATION

The first stage in the (self-)calibration process is to provide an efficient measurement equation which relates the visibilities with the unknown sky and the instrument parameters. In this section, we use the measurement equation presented by Hamaker, Bregman & Sault (1996). For assessing the equation from the array signal processing point of view, the reader is referred to Leshem & van der Veen (2000), Boonstra & van der Veen (2003) and van der Tol, Jeffs & van der Veen (2007).

We assume that we have a radio interferometer consisting of N receiver antennas. Each antenna consists of two orthogonal dual-polarization feeds, which receive the incident polarized waves from astrophysical sources in the sky. We also assume that the radio frequency sky consists of K discrete, uncorrelated sources. The sources are far enough from the array that their radiations can be assumed to be plane waves.

Let us consider $\boldsymbol{e}_i = [e_{Xi}\ e_{Yi}]^{\mathrm{T}}$ represents the electric field vector of the ith source. This field causes an induced voltage $\tilde{\boldsymbol{v}}_{pi} = [v_{Xpi}\ v_{Ypi}]^{\mathrm{T}}$ at antenna p for every $p \in \{1, 2, \ldots, N\}$ due to

$$\tilde{\boldsymbol{v}}_{pi} = \mathbf{J}_{pi}\boldsymbol{e}_i. \tag{1}$$

In equation (1), the 2×2 Jones matrix $\mathbf{J}_{pi}$ describes the complex interaction between the fields, the antenna beam-shape and ionosphere, as well as the remaining signal path. The total signal at the antenna p, $\boldsymbol{v}_p$, is a linear superposition of K such signals as in (1). At the end, the receiver noise $\boldsymbol{v} = [v_X\ v_Y]^{\mathrm{T}}$ also is added to this signal.

Before correlating the voltages of the interferometer antennas, each voltage is corrected for a geometric delay depending on the location of its receiver antenna on the Earth. Thereafter, the pth antenna voltage gets correlated to the other $N - 1$ array antenna voltages in the array correlator. The correlated voltages, referred to as *visibilities* (Hamaker et al. 1996) of the baseline pq corresponding to the pth and the qth antennas, $E\{\boldsymbol{v}_p \otimes \boldsymbol{v}_q^{\mathrm{H}}\}$, can be given as

$$\mathbf{V}_{pq} = \sum_{i=1}^{K} \mathbf{J}_{pi}(\boldsymbol{\theta})\mathbf{C}_i\mathbf{J}_{qi}^{\mathrm{H}}(\boldsymbol{\theta}) + \mathbf{N}_{pq}, \quad p, q \in \{1, 2, \ldots, N\}. \tag{2}$$

In equation (2), the Jones matrices (Hamaker et al. 1996), $\mathbf{J}_{pi}(\boldsymbol{\theta})$ and $\mathbf{J}_{qi}(\boldsymbol{\theta})$ describe the electromagnetic interaction of the source i

at antennas p and q, respectively (Born & Wolf 1999). In particular, the instrumental properties (the beam shape, low-noise amplifier gain, system frequency response, etc.) as well as the propagation properties (tropospheric and ionospheric distortions, etc.) are represented by the Jones matrix formalism. They can be considered as the direction-dependent gains of the corresponding antennas for the ith source. The unknown parameter vector $\boldsymbol{\theta} \in \mathbb{C}^P$ contains the parameters of both the instrument and the sky model. $\mathbf{N}_{pq}$ is the 2×2 noise matrix of the baseline pq. The *coherency* matrix (Hamaker et al. 1996; Born & Wolf 1999) is defined as

$$\mathbf{C}_i = \mathrm{E}\left\{ \boldsymbol{e}_i \otimes \boldsymbol{e}_i^{\mathrm{H}} \right\}, \tag{3}$$

which provides us information about the polarization state of the radiation of the ith source. We assume that an initial estimate of the coherency matrix $\mathbf{C}_i$ is known based on some prior information, about the source or sky properties, obtained by previous observations.

Calibration is essentially a step to estimate the elements of the unknown parameter vector $\boldsymbol{\theta}$, i.e. P complex values or $2P$ real values. The parameter vector $\boldsymbol{\theta}$ is a random variable, that varies as a function of time and frequency, by nature. We assume without loss of generality that we are calibrating on a small enough time and frequency interval during which the variation of $\boldsymbol{\theta}$ is negligible. We then split the integration time to several sub-intervals and apply the calibration process to all of them separately.

Finally, the vectorized form of equation (2) can also be written as

$$\boldsymbol{v}_{pq} \equiv \mathrm{vec}(\mathbf{V}_{pq}) = \sum_{i=1}^{K} \mathbf{J}_{qi}^*(\boldsymbol{\theta}) \otimes \mathbf{J}_{pi}(\boldsymbol{\theta})\mathrm{vec}(\mathbf{C}_i) + \boldsymbol{n}_{pq}, \tag{4}$$

where $\boldsymbol{n}_{pq} = \mathrm{vec}(\mathbf{N}_{pq})$. Ignoring the auto-correlations for $p = q$, and stacking up all cross-correlations as $\boldsymbol{y} = [\boldsymbol{v}_{12}^{\mathrm{T}} \; \boldsymbol{v}_{13}^{\mathrm{T}} \; \ldots \; \boldsymbol{v}_{(N-1)N}^{\mathrm{T}}]^{\mathrm{T}}$, and all noise vectors as $\boldsymbol{n} = [\boldsymbol{n}_{12}^{\mathrm{T}} \; \boldsymbol{n}_{13}^{\mathrm{T}} \; \ldots \; \boldsymbol{n}_{(N-1)N}^{\mathrm{T}}]^{\mathrm{T}}$, we obtain the general form of the measurement equation as

$$\boldsymbol{y} = \sum_{i=1}^{K} \boldsymbol{s}_i(\boldsymbol{\theta}) + \boldsymbol{n}. \tag{5}$$

In equation (5), $\boldsymbol{y}, \boldsymbol{n} \in \mathbb{C}^M$, where M is at most $2N(N-1)$ providing all the cross-correlations. The dimension of the parameter vector $\boldsymbol{\theta}$, P, is a multiple of KN. Thus, for a large enough N and a small enough K, there are enough constraints for estimating $\boldsymbol{\theta}$. However, when the number of sources in the sky is uncertain, the optimal K could be selected using Aikaike's Information Criterion (AIC; Akaike 1973) as presented in Yatawatta et al. (2009). The non-linear function $\boldsymbol{s}_i(\boldsymbol{\theta})$, defined for $i \in \{1, 2, \ldots, K\}$ as

$$\boldsymbol{s}_i(\boldsymbol{\theta}) \equiv \begin{bmatrix} \mathbf{J}_{2i}^*(\boldsymbol{\theta}) \otimes \mathbf{J}_{1i}(\boldsymbol{\theta})\mathrm{vec}(\mathbf{C}_i) \\ \mathbf{J}_{3i}^*(\boldsymbol{\theta}) \otimes \mathbf{J}_{1i}(\boldsymbol{\theta})\mathrm{vec}(\mathbf{C}_i) \\ \vdots \\ \mathbf{J}_{Ni}^*(\boldsymbol{\theta}) \otimes \mathbf{J}_{(N-1)i}(\boldsymbol{\theta})\mathrm{vec}(\mathbf{C}_i) \end{bmatrix},$$

corresponds to the contribution of the ith source in the observation. The noise $\boldsymbol{n}$ is assumed to have a multivariate Gaussian distribution with zero mean and $M \times M$ covariance matrix $\boldsymbol{\Pi}$, i.e. $\boldsymbol{n} \sim \mathcal{N}(0, \boldsymbol{\Pi})$ (Yatawatta et al. 2009). Having the measurement equation in hand, one can apply different calibration techniques for estimating the ML of the unknowns.

3 THE LS, EM AND THE SAGE CALIBRATION ALGORITHMS

In this section, we briefly discuss the LS (Normal) calibration via the LM algorithm. We also discuss the new robust calibration techniques, the EM and in particular the SAGE calibration algorithms.

3.1 The LS calibration via LM algorithm

LS calibration considers the additive noise $\mathcal{N}$ to be a white Gaussian noise. Because the measurement equation shown in equation (5) has the general form of a non-linear regression model (Gallant 1975; Bates & Watts 2007), the likelihood of the unknown parameter $\boldsymbol{\theta}$ is maximized when the sum of squared residuals is minimized. Thus, the ML estimation of $\boldsymbol{\theta}$ will be equal to the below least squared error estimation

$$\widehat{\boldsymbol{\theta}} = \arg\min_{\boldsymbol{\theta}} \left\| \boldsymbol{y} - \sum_{i=1}^{K} \boldsymbol{s}_i(\boldsymbol{\theta}) \right\|^2. \tag{6}$$

It is equivalent to minimize the distance between the observed visibilities in $\boldsymbol{y}$, and the predicted interferometer response as a superposition of K non-linear functions $\boldsymbol{s}_i(\boldsymbol{\theta})$ for $i \in \{1, 2, \ldots, K\}$. However, solving equation (6) suffers the same set of problems faced by any non-linear optimization problem, such as convergence to a local minimum, having a slow speed of convergence and significant computational cost.

There are various gradient-based optimization algorithms for estimating $\widehat{\boldsymbol{\theta}}$ at equation (6). The iterative LM algorithm is one of the most robust gradient-based optimization techniques in the sense that most of the time, given suitable initial suggestion $\boldsymbol{\theta}^0$, it converges to a global optimum. Considering $\phi(\boldsymbol{\theta}) = ||\boldsymbol{y} - \sum_{i=1}^{K} \boldsymbol{s}_i(\boldsymbol{\theta})||^2$ as the cost function, the estimation of $\boldsymbol{\theta}$ at the $(k+1)$th iteration of the algorithm will be obtained by

$$\boldsymbol{\theta}^{k+1} = \boldsymbol{\theta}^k - \left(\nabla_{\boldsymbol{\theta}} \nabla_{\boldsymbol{\theta}}^{\mathrm{T}} \phi(\boldsymbol{\theta}) + \lambda \mathbf{H} \right)^{-1} \nabla_{\boldsymbol{\theta}} \phi(\boldsymbol{\theta})|_{\boldsymbol{\theta}^k}. \tag{7}$$

In equation (7), $\nabla_{\boldsymbol{\theta}}$ is the gradient with respect to $\boldsymbol{\theta}$, and λ is the damping factor which should be adjusted at each iteration (Lampton 1997). The matrix $\mathbf{H} = \mathrm{diag}(\nabla_{\boldsymbol{\theta}} \nabla_{\boldsymbol{\theta}}^{\mathrm{T}} \phi(\boldsymbol{\theta}))$ is the diagonal of the Hessian matrix.

The EM algorithm and, in particular, the SAGE algorithm improve the accuracy and computational cost compared with the LS calibration. Since they break the ML estimation problem into smaller problems, the computational cost will be decreased by an order of magnitude and the rate of convergence is substantially increased.

3.2 The EM calibration algorithm

In order to apply the EM algorithm (Feder & Weinstein 1988) in calibration, we first need to extract a complete data space $\boldsymbol{x}$ from the observed data $\boldsymbol{y}$. Similar to Yatawatta et al. (2009), we consider the complete data space as $\boldsymbol{x} = [\boldsymbol{x}_1^{\mathrm{T}} \; \boldsymbol{x}_2^{\mathrm{T}} \; \ldots \; \boldsymbol{x}_K^{\mathrm{T}}]^{\mathrm{T}}$ in which $\boldsymbol{x}_i$ has the definition

$$\boldsymbol{x}_i \equiv \boldsymbol{s}_i(\boldsymbol{\theta}_i) + \boldsymbol{n}_i, \quad \text{for } i \in \{1, 2, \ldots K\}. \tag{8}$$

In fact, equation (8) assumes that the contribution of the ith source in the observation depends only on a subset of parameters, $\boldsymbol{\theta}_i$. So, we partition the unknowns over the parameter vector $\boldsymbol{\theta}$ corresponding to all the K sources in the sky as $\boldsymbol{\theta} = [\boldsymbol{\theta}_1^{\mathrm{T}} \; \boldsymbol{\theta}_2^{\mathrm{T}} \; \ldots \; \boldsymbol{\theta}_K^{\mathrm{T}}]^{\mathrm{T}}$. This partitioning is justifiable as each source is at a unique direction on the sky, and for each antenna, the signal path of all sources

is the same. This is the case for our initial assumption where the sources are separated sufficiently. Also, the total noise is arbitrary decomposed into K components, $\boldsymbol{n}_i$ for $i \in \{1, 2, \ldots, K\}$, such that

$$\boldsymbol{n} = \sum_{i=1}^{K} \boldsymbol{n}_i. \tag{9}$$

As the most convenient assumption, we let the noise components $\boldsymbol{n}_i$s to follow statistically independent zero mean Gaussian distributions with the covariance matrix

$$\mathrm{E}\left\{\boldsymbol{n}_i \boldsymbol{n}_j^{\mathrm{H}}\right\} = \beta_i \delta_{ij} \boldsymbol{\Pi}, \tag{10}$$

where

$$\beta_i \in [0, 1], \quad \text{for } i \in \{1, 2, \ldots, K\}, \quad \sum_{i=1}^{K} \beta_i = 1. \tag{11}$$

In principle, we can associate stronger sources with higher noise, hence higher β_is, and vice versa.

Combining equation (5) and equation (8), the observed data $\boldsymbol{y}$ will be derived from

$$\boldsymbol{y} = \sum_{i=1}^{K} \boldsymbol{x}_i. \tag{12}$$

Therefore, for the given complete data space $\boldsymbol{x}$ we have

$$\boldsymbol{y} = [\mathbf{I}\ \mathbf{I}\ \ldots\ \mathbf{I}]\boldsymbol{x} = \mathbf{G}\boldsymbol{x}, \tag{13}$$

where $\mathbf{G}$ is a block matrix containing the identity matrix $\mathbf{I}$ for K times.

Having the definitions of complete and observed data in hand, the EM algorithm can be used to estimate the ML of the parameter vector $\boldsymbol{\theta}$. Applying the EM method for the new form of the measurement equation, equation (13), the below Expectation (E) and Maximization (M) steps are developed at the $(k + 1)$th iteration for $i \in \{1, 2, \ldots, K\}$.

E Step: calculating the conditional mean $\widehat{\boldsymbol{x}}_i^k = \mathrm{E}\{\boldsymbol{x}_i | \boldsymbol{y}, \boldsymbol{\theta}^k\}$. Considering the fact that $\boldsymbol{x}$ and $\boldsymbol{y}$ are jointly Gaussian we get

$$\widehat{\boldsymbol{x}}_i^k = \boldsymbol{s}_i\left(\boldsymbol{\theta}_i^k\right) + \beta_i \left(\boldsymbol{y} - \sum_{l=1}^{K} \boldsymbol{s}_l\left(\boldsymbol{\theta}_l^k\right)\right). \tag{14}$$

M Step: finding $\boldsymbol{\theta}_i^{k+1}$ such that minimizes the cost function $\phi(\boldsymbol{\theta}_i) = ||[\widehat{\boldsymbol{x}}_i^k - \boldsymbol{s}_i(\boldsymbol{\theta}_i)](\beta_i \boldsymbol{\Pi})^{-1/2}||^2$ with respect to $\boldsymbol{\theta}_i$. This is also a non-linear optimization problem where the LM technique can be applied. The result is given by

$$\boldsymbol{\theta}_i^{k+1} = \boldsymbol{\theta}_i^k - \left(\boldsymbol{\nabla}_{\boldsymbol{\theta}_i} \boldsymbol{\nabla}_{\boldsymbol{\theta}_i}^{\mathrm{T}} \phi(\boldsymbol{\theta}_i) + \lambda \mathbf{H}_i\right)^{-1} \boldsymbol{\nabla}_{\boldsymbol{\theta}_i} \phi(\boldsymbol{\theta}_i)|_{\boldsymbol{\theta}_i^k}, \tag{15}$$

where $\mathbf{H}_i = \mathrm{diag}(\boldsymbol{\nabla}_{\boldsymbol{\theta}_i} \boldsymbol{\nabla}_{\boldsymbol{\theta}_i}^{\mathrm{T}} \phi(\boldsymbol{\theta}_i))$.

We repeat the above two steps starting from iteration $k = 1$ until convergence or an upper limit which has been reached. Since at each iteration, i goes from 1 to K, the solutions of each source will be updated. In Appendix A1, we derive the EM algorithm for the problem in details and the results given above.

3.3 The SAGE calibration algorithm

SAGE algorithm (Fessler & Hero 1994) performs better than the EM algorithm and has a higher speed of convergence and solution accuracy. The major difference between these two approaches is in the way of assigning the noise to the complete data space.

Similar to applying the classical EM algorithm, the first step in the SAGE algorithm is to find a complete data space relating the observations to the unknown parameters. For this purpose, consider the set of all indices related to all the K sources as

$$P = \{1, 2, \ldots, K\}. \tag{16}$$

Then, define index sets W_i such that

$$\varnothing \neq W_i \subsetneq P, \tag{17}$$

where for all $a, b \in W_i$, we have $a \neq b$, and the sources corresponding to the indexes a and b, source a and source b, have a small angular distance (they are near to each other in the sky) and subsequently they share some elements of the parameter vector $\boldsymbol{\theta}$. We have

$$W_i \cap W_j = \varnothing, \quad \text{for } i \neq j. \tag{18}$$

Let us assume that we have m such index sets. Thus,

$$m \leq K, \quad P = \bigcup_{i=1}^{m} W_i. \tag{19}$$

For each $i \in \{1, 2, \ldots, m\}$, we define a new parameter vector $\boldsymbol{\theta}_{W_i}$ consisting of all the elements in the parameter vector $\boldsymbol{\theta}$, which are affected by the sources with indexes in W_i. In other words, we provide the possibility to have elements in these new parameter vectors which are shared by more than one source.

Now, we make a new partitioning over the parameter vector $\boldsymbol{\theta}$ as

$$\boldsymbol{\theta} = \left[\boldsymbol{\theta}_{W_1}^{\mathrm{T}}\ \boldsymbol{\theta}_{W_2}^{\mathrm{T}}\ \cdots\ \boldsymbol{\theta}_{W_m}^{\mathrm{T}}\right]^{\mathrm{T}}. \tag{20}$$

Similar to Fessler & Hero (1994), we define the hidden data space $\boldsymbol{x}_{W_i}$ as

$$\boldsymbol{x}_{W_i} = \sum_{l \in W_i} \boldsymbol{s}_l(\boldsymbol{\theta}_{W_i}) + \boldsymbol{n}, \tag{21}$$

selecting the index set $W_i \in \{W_1, W_2, \ldots, W_m\}$ which preferably consists of the indices of the brightest sources. Note that in equation (21) all the noise has been associated with the sources with indices in W_i. This is the main difference between the SAGE and the classical EM algorithm. Using equation (21), the measurement equation can be written as

$$\boldsymbol{y} = \boldsymbol{x}_{W_i} + \sum_{\substack{j=1 \\ j \neq i}}^{m} \sum_{l \in W_j} \boldsymbol{s}_l(\boldsymbol{\theta}_{W_j}). \tag{22}$$

By applying the EM algorithm to this new form of the measurement equation, we arrive at the following steps for the $(k + 1)$th iteration of the SAGE approach:

SAGE E Step: computing the conditional mean $\widehat{\boldsymbol{x}}_{W_i}^k = \mathrm{E}\{\boldsymbol{x}_{W_i} | \boldsymbol{y}, \boldsymbol{\theta}^k\}$. Since $\boldsymbol{x}_{W_i}$ and $\boldsymbol{y}$ are also jointly Gaussian, we get

$$\begin{aligned}
\widehat{\boldsymbol{x}}_{W_i}^k &= \sum_{l \in W_i} \boldsymbol{s}_l\left(\boldsymbol{\theta}_{W_i}^k\right) + \left(\boldsymbol{y} - \sum_{j=1}^{m} \sum_{l \in W_j} \boldsymbol{s}_l\left(\boldsymbol{\theta}_{W_j}^k\right)\right) \\
&= \boldsymbol{y} - \sum_{\substack{j=1 \\ j \neq i}}^{m} \sum_{l \in W_j} \boldsymbol{s}_l\left(\boldsymbol{\theta}_{W_j}^k\right).
\end{aligned} \tag{23}$$

SAGE M Step: finding $\boldsymbol{\theta}_{W_i}^{k+1}$ which is minimizing the cost function $\phi_{W_i}(\boldsymbol{\theta}_{W_i}) = ||[\widehat{\boldsymbol{x}}_{W_i}^k - \sum_{l \in W_i} \boldsymbol{s}_l(\boldsymbol{\theta}_{W_i})](\boldsymbol{\Pi})^{-1/2}||^2$ with respect to $\boldsymbol{\theta}_{W_i}$. The result is similar to equation (15). As before, we iterate from $k = 1$ to an upper limit. At each iteration, we change the index set W_i within $\{W_1, W_2, \ldots, W_m\}$ to update all or some sources.

A special case of the SAGE algorithm was presented by Yatawatta et al. (2009) if we consider $W_i = \{i\}$ for all $i \in \{1, 2, \ldots, K\}$. In fact, we apply the same partitioning over the unknown parameter $\boldsymbol{\theta}$ which is used for the classical EM algorithm, $\boldsymbol{\theta} = [\boldsymbol{\theta}_1^{\mathrm{T}}\ \boldsymbol{\theta}_2^{\mathrm{T}} \ldots \boldsymbol{\theta}_K^{\mathrm{T}}]^{\mathrm{T}}$. By choosing the index i, where the source i is preferably the brightest source in the sky, the hidden data space will be defined by

$$\boldsymbol{x}_i = \boldsymbol{s}_i(\boldsymbol{\theta}_i) + \boldsymbol{n}. \tag{24}$$

Equation (24) gives us the definition of the observed data as

$$\boldsymbol{y} = \boldsymbol{x}_i + \sum_{\substack{l=1 \\ l \neq i}}^{K} \boldsymbol{s}_l(\boldsymbol{\theta}_l), \tag{25}$$

and, subsequently applying the EM on the measurement equation, the $(k+1)$th iteration of the SAGE technique will be as below:

SAGE E Step: conditional mean $\widehat{\boldsymbol{x}}_i^k = \mathrm{E}\{\boldsymbol{x}_i | \boldsymbol{y}, \boldsymbol{\theta}^k\}$ is derived from

$$\widehat{\boldsymbol{x}}_i^k = \boldsymbol{s}_i\left(\boldsymbol{\theta}_i^k\right) + \left(\boldsymbol{y} - \sum_{l=1}^{K} \boldsymbol{s}_l\left(\boldsymbol{\theta}_l^k\right)\right) = \boldsymbol{y} - \sum_{\substack{l=1 \\ l \neq i}}^{K} \boldsymbol{s}_l\left(\boldsymbol{\theta}_l^k\right). \tag{26}$$

SAGE M Step: $\boldsymbol{\theta}_i^{k+1}$ is given by minimizing the cost function $\phi_i(\boldsymbol{\theta}_i) = ||[\widehat{\boldsymbol{x}}_i^k - \boldsymbol{s}_i(\boldsymbol{\theta}_i)](\boldsymbol{\Pi})^{-1/2}||^2$.

In Appendix A2, we present the complete calculation process of applying the SAGE algorithm to the calibration problem.

3.4 Computational cost

At each iteration of the LS calibration scheme via the LM algorithm, the non-linear system presented by equation (7) should be solved which is of order (KN). Therefore, ignoring the cost of calculations for the inverse part in this equation, the computational cost will be $\mathcal{O}((KN)^2)$. Furthermore, for radio synthesis arrays such as LOFAR and SKA, computing the matrix inverse in equation (7) is very costly since the number of measured data is becoming very large. While, at each iteration of the EM algorithm, we should solve equation (15) K times and subsequently the computational cost of the EM calibration algorithm will be $K\mathcal{O}(N^2)$, which is still much cheaper compared with the LS calibration approach. Thus, the EM as well as the SAGE calibration techniques is superior to the LS one in terms of computational cost.

Note that the LM optimization technique is employed for all the LS, EM and the SAGE calibration algorithms. Thus, its corresponding inversion computation is shared in all the methods. However, in the EM and SAGE algorithms the size of the matrix that is inverted is smaller compared to that of the LS algorithm because of the partitioning procedure of the parameters. Given the fact that the computational complexity of the matrix inversion scales a number of its elements to the third power, it is evident that inverting few smaller matrices as in the EM and SAGE cases is faster than inverting a single large matrix, which is the case for the LS algorithm.

4 NOISE IN SOLUTIONS

To compare the accuracy of the SAGE calibration scheme to the LS one, we statistically analyse the solver noise. The lower the solver noise in a calibration method, the smaller the errors in calibrated solutions provided by the calibration algorithm itself. Consequently, the accuracy of the method is higher.

In order to do a proper statistical analysis of the calibration algorithm's solver noise, we make the assumption that their solutions are linear combinations of a deterministic trend and noise. This noise can have many origins. In the ideal case, it is introduced by the primary noise sources (thermal noise at the receiver, the sky noise, radio interference, etc.) and by variations of the instrumental and propagation properties. However, in reality the solver noise, which we are most concerned about and is introduced by the calibration method itself, is also added to those sources.

The goal in this section is to quantify the level of the solver noise for the different calibration algorithms, based on the evaluation of the statistical interaction between their solutions.

4.1 Statistical similarity

In order to compare the level of solver noise for the different calibration methods, we assume that the true values of the solutions from different directions at the same antenna are statistically uncorrelated. Therefore, any correlation between the calibrated solutions for different directions is caused by the corresponding calibration technique itself. In reality, there are also correlations that originate from the system noise in the solutions, but this can be ignored when we compare the solutions of a fixed measured data obtained by different calibration methods. Therefore, a high solver noise in a calibration scheme causes strongly correlated solutions for any number of directions at one given antenna (or maybe even more). To detect the statistical similarity between the gain solutions we proceed as follows.

Once we estimate the parameter vector $\boldsymbol{\theta}$, we obtain the Jones matrices $\mathbf{J}_{qs}(\boldsymbol{\theta})$ for different antennas $q \in \{1, 2, \ldots, N\}$ and different directions $s \in \{1, 2, \ldots, K\}$. Let us consider the matrices to be diagonal as

$$\mathbf{J}_{qs} = \begin{bmatrix} J_{11,q} & 0 \\ 0 & J_{22,q} \end{bmatrix}_s, \tag{27}$$

where $J_{11,q}$ and $J_{22,q}$ are complex values. We treat each gain solution from the direction s of antenna q as a random vector $\boldsymbol{\theta}_{qs}$ defined by

$$\boldsymbol{\theta}_{qs} = [\mathfrak{Re}(J_{11,q})\ \mathfrak{Im}(J_{11,q})\ \mathfrak{Re}(J_{22,q})\ \mathfrak{Im}(J_{22,q})]_s^{\mathrm{T}}. \tag{28}$$

Now, we can investigate the statistical similarity between the gain solutions utilizing KLD and LRT. In general, both KLD and LRT compare the efficiency of fitting two different statistical models to a fixed set of measurements. Utilizing these methods on the random vectors defined by equation (28), we obtain their statistical similarity in two different interpretations. The higher these similarities, the higher the interaction between the solutions, as well as the solver noise.

4.2 Kullback–Leibler Divergence

An efficient way to quantify the statistical similarity between the solutions is to use KLD.

The relative entropy, defined as the KLD, for each couple of probability density functions (PDFs) f and g of solutions $\boldsymbol{\theta}_{qk}$ and $\boldsymbol{\theta}_{ql}$, respectively, is defined as

$$\mathrm{KLD}(f, g) \equiv \sum_{\boldsymbol{\theta}_{qk}} f(\boldsymbol{\theta}_{qk}) \log \frac{f(\boldsymbol{\theta}_{qk})}{g(\boldsymbol{\theta}_{qk})}, \tag{29}$$

where the solutions are corresponding to the given antenna q at the two different directions k and l.

The KLD is a measure of information 'divergence' between two different PDFs for the same random variable. Larger values of KLD(f, g) are interpreted as less interaction between the solutions, and subsequently, as less solver noise. We use a Monte Carlo method to evaluate equation (29).

4.2.1 Density estimation

To calculate the value of KLD we need to estimate the PDFs of the solutions.

We define the PDF of the random vector $\boldsymbol{\theta}_{qs}$, $f(\boldsymbol{\theta}_{qs}; \boldsymbol{\beta})$, as a mixture of L isotropic (scalar variance) Gaussian PDFs. The assumption of mixture modelling is based on the fact that the solutions are affected by parameters that belong to different underlying statistical

populations and due to the Central Limit Theorem it is reasonable to assume that the distributions of those populations converge to Gaussian distributions. Therefore, it can be written as

$$f(\boldsymbol{\theta}_{qs}, \boldsymbol{\beta}) = \sum_{l=1}^{L} p_l g(\boldsymbol{\theta}_{qs}; \boldsymbol{m}_l, \sigma_l), \tag{30}$$

where $g(\boldsymbol{\theta}_{qs}; \boldsymbol{m}_l, \sigma_l)$ is the PDF of a four-dimensional Gaussian distribution with mean $\boldsymbol{m}_l$ and variance $\sigma_l^2 \mathbf{I}$ given by

$$g(\boldsymbol{\theta}_{qs}; \boldsymbol{m}_l, \sigma_l) = \frac{1}{(\sqrt{2\pi}\sigma_l)^4} exp\left(-\frac{1}{2}\left(\frac{\|\boldsymbol{\theta}_{qs} - \boldsymbol{m}_l\|}{\sigma_l}\right)^2\right), \tag{31}$$

and $\boldsymbol{\beta}$ is the vector of the mixture model unknown parameters

$$\boldsymbol{\beta} = \left[p_1, \boldsymbol{m}_1^{\mathrm{T}}, \sigma_1, \ldots, p_L, \boldsymbol{m}_L^{\mathrm{T}}, \sigma_L\right]^{\mathrm{T}}, \tag{32}$$

which are estimated by the EM algorithm (Bilmes 1998).

4.2.2 Akaike's Information Criterion for model order selection

To find the optimum number of L (the order of Gaussian mixture model in equation 30) we use AIC (Akaike 1973).

According to the definition of AIC, we select an L such that it gives us the minimum value of AIC(L) which is defined as

$$\mathrm{AIC}(L) = -2\mathrm{L}(\widehat{\boldsymbol{\beta}}) + 2k, \tag{33}$$

where $L(\cdot)$ is the log-likelihood function of $\boldsymbol{\theta}$, $\widehat{\boldsymbol{\beta}}$ is the ML estimate of $\boldsymbol{\beta}$ and k is the number of parameters in the model presented by equation (30).

4.3 Likelihood-ratio test

Another standard approach to investigate the statistical interaction between the solutions is the LRT. Using this test, we can compare two models, which both can be fitted to our solutions.

Let us define for each antenna q, where $q \in \{1, 2, \ldots, N\}$, and each pair of directions like k and l, where $k, l \in \{1, 2, \ldots, K\}$, a new random vector z_{qkl} as

$$z_{qkl} = \left[\boldsymbol{\theta}_{qk}^{\mathrm{T}} \, \boldsymbol{\theta}_{ql}^{\mathrm{T}}\right]^{\mathrm{T}}. \tag{34}$$

In fact, we are concatenating the solutions of the same antenna for two different directions together. Assume that z_{qkl} is following a multivariate Gaussian distribution with mean

$$\boldsymbol{m} = \left[\bar{\boldsymbol{m}}(\boldsymbol{\theta}_{qk})^{\mathrm{T}} \, \bar{\boldsymbol{m}}(\boldsymbol{\theta}_{ql})^{\mathrm{T}}\right]^{\mathrm{T}}, \tag{35}$$

and the 8×8 variance matrix

$$\boldsymbol{\Sigma_0} = \begin{bmatrix} \mathbf{s}^2(\boldsymbol{\theta}_{qk}) & \mathbf{0} \\ \mathbf{0} & \mathbf{s}^2(\boldsymbol{\theta}_{ql}) \end{bmatrix}, \tag{36}$$

where $\bar{\boldsymbol{m}}$ and $\mathbf{s}^2$ are the sample mean and sample variance of the solutions, respectively. The structure of the variance matrix $\boldsymbol{\Sigma_0}$ tells us that the statistical correlation between the components of the random vector z_{qkl}, or between the solutions $\boldsymbol{\theta}_{qk}$ and $\boldsymbol{\theta}_{ql}$, is zero. This is exactly the desirable case in which the solver noise vanishes. Thus, we can consider this model as our null H_0 model defined by

$$H_0 : z_{qkl} \sim \mathcal{N}(\boldsymbol{m}, \boldsymbol{\Sigma_0}). \tag{37}$$

To investigate the validity of the null model compared with the case in which there exist some correlation between the solutions due to the presence of solver noise, we define the alternative H_1 model as

$$H_1 : z_{qkl} \sim \mathcal{N}(\boldsymbol{m}, \boldsymbol{\Sigma_1}), \tag{38}$$

where the variance matrix $\boldsymbol{\Sigma_1}$ is given by

$$\boldsymbol{\Sigma_1} = \begin{bmatrix} \mathbf{s}^2(\boldsymbol{\theta}_{qk}) & \mathbf{Q}(\boldsymbol{\theta}_{qk}, \boldsymbol{\theta}_{ql}) \\ \mathbf{Q}(\boldsymbol{\theta}_{qk}, \boldsymbol{\theta}_{ql})^{\mathrm{T}} & \mathbf{s}^2(\boldsymbol{\theta}_{ql}) \end{bmatrix}, \tag{39}$$

and the 4×4 matrix $\mathbf{Q}(\boldsymbol{\theta}_{qk}, \boldsymbol{\theta}_{ql})$ denotes the sample covariance of the solutions.

Using the above models, the likelihood ratio is defined as

$$\Lambda = -2\ln\left(\frac{\text{likelihood for null model}}{\text{likelihood for alternative model}}\right), \tag{40}$$

which has a χ^2 distribution with 16 degrees of freedom. As Λ becomes smaller, the null model, in which the statistical correlation as well as the statistical similarity between the solutions is zero, becomes more acceptable compared to the alternative one. Therefore, the smallest the Λ, the less the solver noise and vice versa.

Note that the test result is reliable only when a large number of sample solutions are in hand. In this case, because of the Central Limit Theorem, the distribution of solutions tends to be a multivariate LS distribution, which is assumed initially by the test.

5 ILLUSTRATIVE EXAMPLES

5.1 Simulated observation

First we use a simulated observation to compare the efficiency of the SAGE calibration algorithm with the LS algorithm. Utilizing simulations instead of real observations has the advantage of having the true underlying gains available, which is a luxury not available with real data. Therefore, assessing the convergence of the calibration techniques as well as comparing the accuracy between different calibrated solutions is much more objective.

We consider a linear, east–west radio synthesis array that has 14 dipoles with dual polarization. We put three bright sources in our sky model named A, B and C with intensities 2950, 2900 and 2700 Jy, and three other weak sources named D, E and F with intensities 4, 3.5 and 3 Jy, respectively. The simulated single channel image at 355 MHz is shown in Fig. 1. As we can see in Fig. 1, the weak sources are not visible in the image. We also consider that there is no beam pattern, therefore the whole sky is being observed with uniform sensitivity.

As it is shown in equation (2), in the measured visibilities, the coherency of the sources are multiplied by the Jones matrices (gain errors). We consider the matrices to be diagonal. It means that the signal received at each dipole is not affected by the other one which is an ideal case. We produce gain errors in the norm and phase of the Jones matrices diagonal terms which are 1 and 0 initially. We generate the norm and the phase of the gains as multiplications of random numbers with different linear combinations of *sin* and *cos* functions, whose gradients increase with time. We also add another random term increasing as a function of time, just to the phase errors, to provide the phases with positive and negative slopes. The simulated result is presented by Fig. 2.

Finally, we apply the SAGE and the LS calibration to solve only for the gains of the visible strong sources A, B and C. The residuals of the SAGE and LS calibration using nine iterations are shown in Figs 3 and 4, respectively.

As we can see in Figs 3 and 4, the strong sources are completely removed and the three weak sources are visible in the residuals of the both algorithms which mean both are converging to real solutions. But, the weak source intensities in the residuals of the SAGE calibration are closer to the absolute intensities in our sky
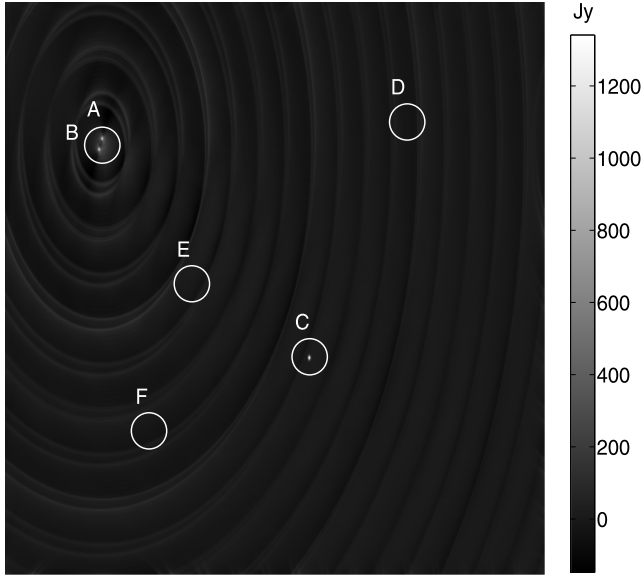
Figure 1. Single channel simulated observation of three bright sources, A, B and C, and three weak sources, D, E and F. The intensity of the bright sources are 2950, 2900 and 2700 Jy and of the weak sources are 4, 3.5 and 3 Jy, respectively. The image size is 8° by 8° at 355 MHz. There are no gain errors and noise in the simulation.
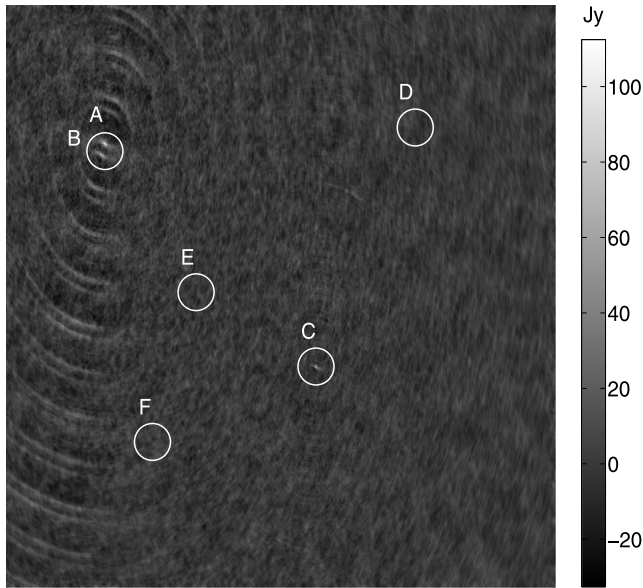

Figure 2. Simulated observation with added gain errors. The errors are complex numbers having norms and phases as multiplications of random numbers with various linear combinations of *sin* and *cos* functions. The gradients of the errors increase as a function of time and the phases are in different negative and positive slopes.

model which shows the superiority of the SAGE calibration in terms of accuracy. This fact is shown more clearly by Table 1 where the real intensities of the weak sources are compared with the calibrated ones.

Note that as this is a single channel simulated observation without any additive noise, the difference between the two method's residuals is slight. However, the importance of applying the SAGE instead of LS calibration is evident since the computational cost of the SAGE is much smaller, as it is discussed in Section 3.4.
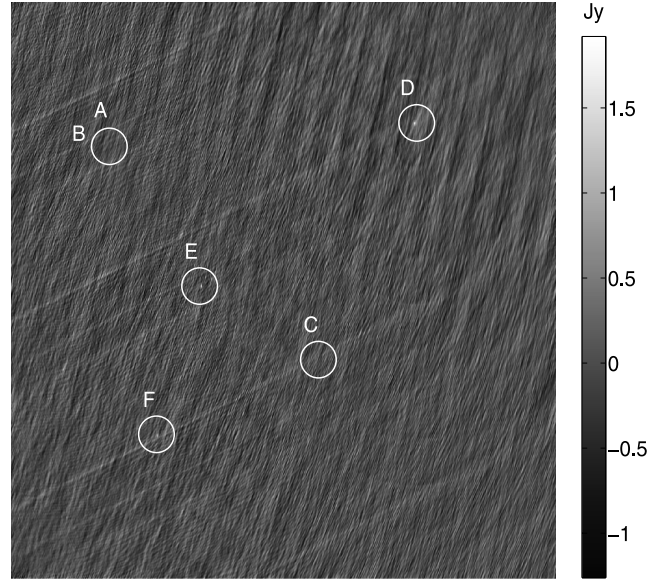
Figure 3. Residual image of the SAGE calibration using nine iterations. The image is only calibrated for the bright sources A, B and C, which are perfectly removed. The weak sources D, E and F appear in the residuals, including source F which is the weakest source in the simulation.
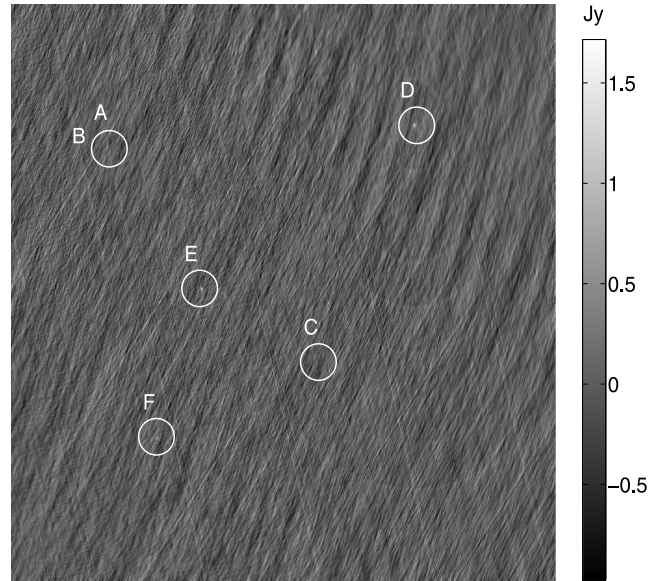

Figure 4. Residual image of the LS calibration using nine iterations. The calibration is processed only for the strong sources A, B and C that are completely removed in the residuals. The two weak sources D and E appear in the image, but the weakest source F is hardly visible.

Fig. 5 shows the performance of the algorithms in terms of accuracy and speed of convergence. As we can see in Fig. 5, the SAGE algorithm's speed of convergence is much higher than that of the standard LS calibration.

In order to investigate the efficiency of the LRT and KLD approaches in revealing the statistical similarity of gain solutions, we applied both methods, using equation 29 and equation 40, to the SAGE and the LS calibration solutions and compared their results with the LRT and KLD of the true Jones parameters (simulated gains). The comparison is shown by Figs 6 and 7. Fig. 6 exhibits an outstanding performance of the LRT approach in which the

Table 1. A comparison of real intensities of the weak sources with the calibrated ones.

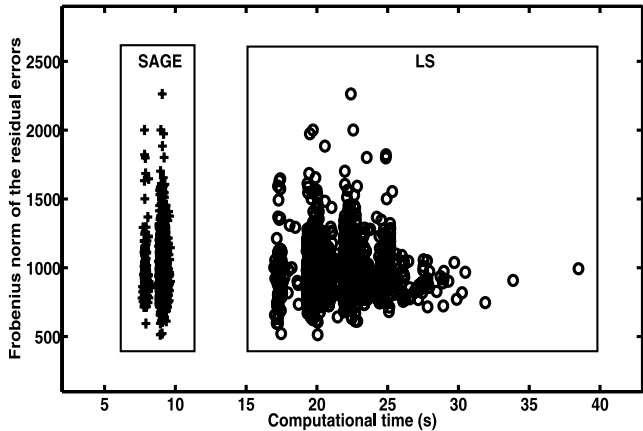| Source	D	E	F
Real intensity(Jy)	4	3.5	3
SAGE calibration	3.8399	3.6695	2.3085
LS calibration	2.8327	2.6329	1.6081

Figure 5. Comparison between the performance of the SAGE and the LS calibrations (nine number of iterations) in order of the accuracy of solutions and the speed of convergence. Different points correspond to different snapshots made from the simulation. The speed of the SAGE calibration technique is higher than the LS calibration, while the norm of their residual errors is almost the same.
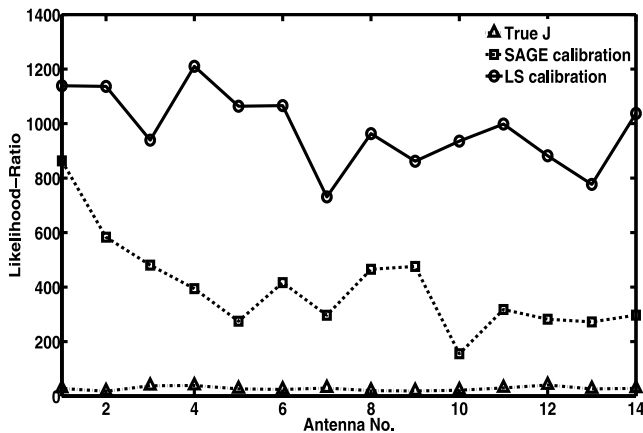
Figure 6. Averaged likelihood ratio of direction-dependent gains (true values and calibrated ones) for all two source combinations between the bright sources A, B and C.

direction dependent gain's lowest statistical similarity belongs to the real Jones values, that is almost zero. For SAGE calibration's solutions this similarity becomes higher, and in LS results it reaches to its highest level. This result demonstrates the superior accuracy of the SAGE calibration's solutions regardless of the residual images. But, the KLD results in Fig. 7 show the same level of statistical correlation in the calibrations' solutions and in the True Jones parameters. This is due to the fact that these results are calculated by Gaussian mixture models, which are fitted to the gains. This characteristic of the KLD approach (using fitted PDFs for gains distributions rather than the true PDFs) decreases the method's sensitivity in revealing
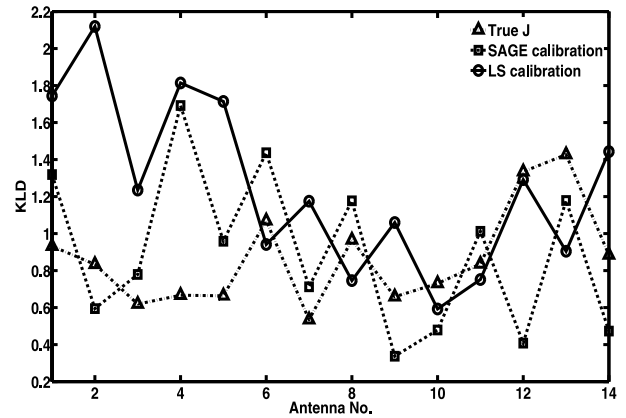
Figure 7. Averaged KLD of direction-dependent gains (true values and calibrated ones) for all two source combinations between the bright sources A, B and C.

the level of statistical similarity between different directions' gains, especially in our case where the simulated gains' correlations are low. However, we anticipate better performance of KLD method in real observations in which the higher gain errors plus additive noise cause a higher solver noise.

5.2 Real observations

To illustrate the applicability of the KLD and LRT approaches in detecting solver noise in real observations calibrated solutions, we use the data from the example in Yatawatta et al. (2009). Yatawatta et al. (2009) present the calibration results using real data obtained during a 24-h long LOFAR test core station (CS1) observation, via SAGE and LS calibration techniques. The one channel images around 3C 461 (Cassiopeia A, CasA) and 3C 401 (Cygnus A, CygA) at 50 MHz after applying these calibration methods using 12 iterations are shown in Fig. 8. The result at Fig. 8 clearly verifies the superiority of the SAGE calibration scheme as it was mentioned in Yatawatta et al. (2009) as well.

We calculate the KLD using equation (29) as well as likelihood ratio using equation (40) for the calibrated solutions of these two sources obtained by the mentioned calibration techniques. In the KLD approach, we fit a Gaussian mixture model, which its components have full rank covariance matrices, to the solutions. The KLD and LRT results are shown in Figs 9 and 10, respectively. As we can see in Fig. 9, the KLD of the solutions derived by the LS calibration is always lower than that of the SAGE calibration. It is also shown in Fig. 10 that the LRT of the LS calibration's solutions is always higher than the SAGE calibration's. Therefore, the solver noise in the LS calibration results is measurably higher than in the solutions obtained by the SAGE calibration. This means that the accuracy of the SAGE calibration is always higher than that of the LS calibration, which is visible in Fig. 8 as well as the aforementioned images in Yatawatta et al. (2009).

6 SUMMARY

Since the new generation of radio synthesis arrays is producing a large amount of data with high sensitivity, it is of great interest to devise new calibration techniques in order to increase the accuracy of solutions with the highest possible speed of convergence.
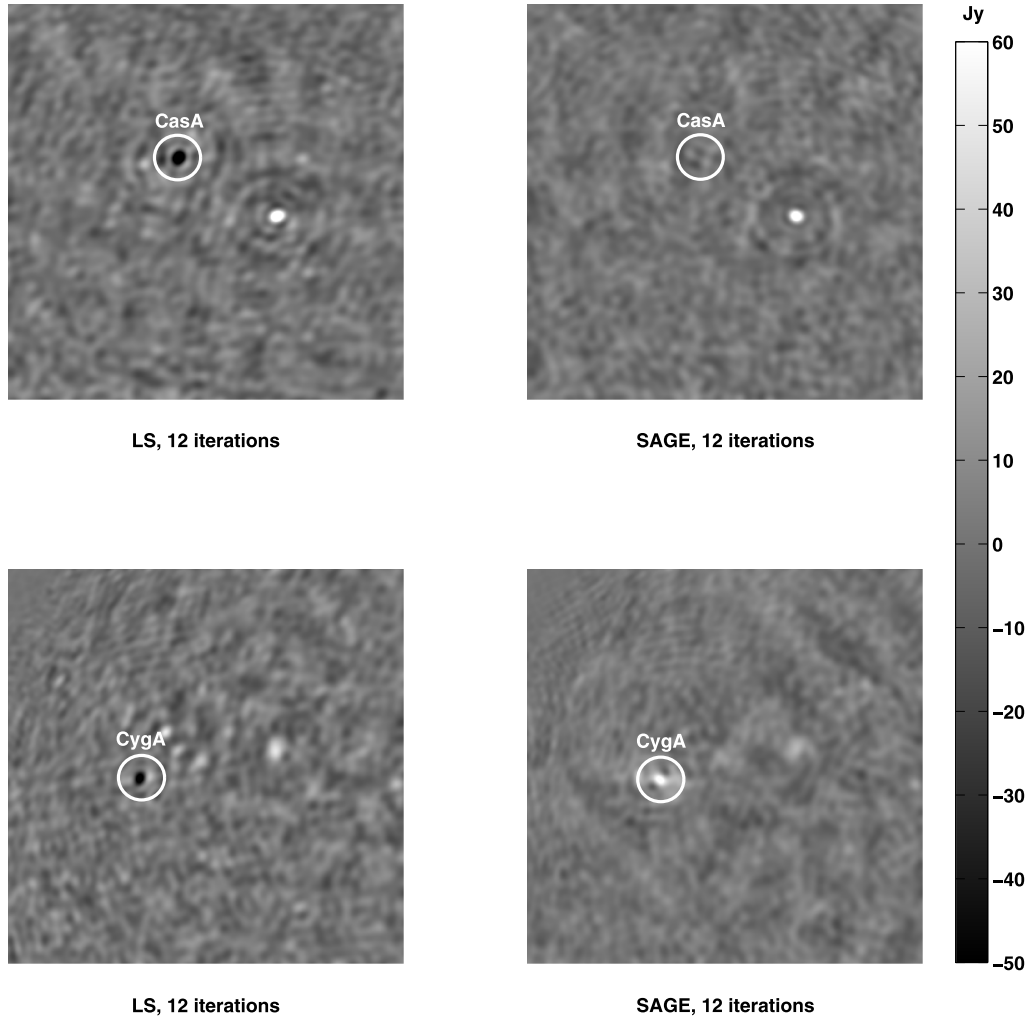
Figure 8. Residual images around CasA (top row) and CygA (bottom row) obtained by the LS calibration (left-hand column) and the SAGE calibration (right-hand column) using 12 iterations. CasA is oversubtracted in the residual of the LS calibration result, due to the inaccuracy in the estimation of the relevant direction-dependent gain, while in the SAGE calibration result it is removed almost perfectly. On the other hand, both the SAGE and the LS calibrations present some problems around CygA since at some point of the integration time it goes very close to the horizon. Even in that case, the subtraction residual for the SAGE algorithm is 10 per cent lower than for the LS method.
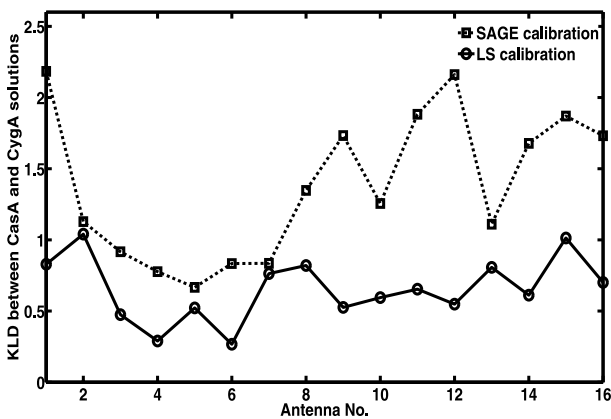

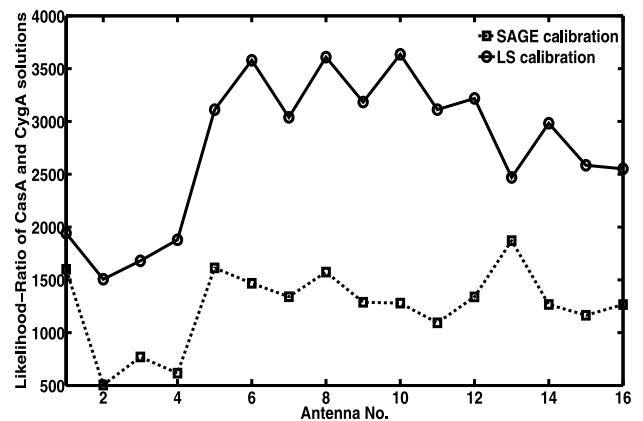**Figure 9.** KLD of the gain solutions for CasA and CygA.

Figure 10. Likelihood ratio of the gain solutions for CasA and CygA.

In this paper, we presented the superior performance of the SAGE calibration scheme compared with the traditional LS calibration method. The superiority is in the sense that SAGE calibration has the highest accuracy, the fastest speed of convergence and the cheap-

est computational cost. Since both the algorithms are estimating the ML of unknowns in different ways, it is possible that in some special cases, such as having a very low initial noise in the measured visibilities, we do not have a specific difference between the accuracy

of their solutions. While, even in this case, the SAGE calibration's faster speed of convergence and cheaper computational cost justify its application instead of the LS calibration. We compared the accuracy and the rate of convergence of the SAGE and the LS calibration in a simulated observation example. More accurate results in a much shorter time are obtained by the SAGE algorithm compared with the LS. The challenge in improving the performance of the SAGE calibration technique is to find the best way of partitioning over the unknown parameter space. This can highly affect both the accuracy and speed of convergence of the calibration process.

On the other hand, there always exists some estimation errors in the calibrated solutions. These errors are originated from the system noise (sky and instrumental) in the measurements, plus 'solver noise' which is referred to errors produced by the calibration algorithm itself. The more accurate the calibrated solutions are, the less the amount of solver noise is. Based on this fact, the best calibration method is the one which provides us with the minimum solver noise. KLD and LRT are utilized to reveal the level of solver noise in the solutions of different calibration schemes. We showed in illustrative examples that the LRT algorithm produces a very promising result. The KLD method is rather inconclusive according to the initial assumption for the PDFs fitted to the solutions. We assumed that the distribution of the solutions is a mixture of Gaussian distributions. However, in reality, the solutions may follow a different distribution and subsequently the KLD result may not have the same efficiency as the LRT's. Therefore, initially we should find the proper distribution which is appropriate for the solutions in order to calculate the KLD.

The main direction of future work should be to investigate the application of the proposed calibration technique to real data obtained by LOFAR. Since LOFAR is observing the whole sky, the number of radio sources in the sky model will be very large. Subsequently, for applying the SAGE calibration, partitioning over the unknowns by manually checking the characteristics of all the sources will not be efficient. Therefore, the first challenge in utilizing the SAGE calibration to real data would be automating the partitioning over the unknowns for any given problem. Furthermore, we saw in the paper that all the mentioned calibration algorithms involve essentially the solution of a non-linear optimization problem. Applying suitable regularization techniques using proper smoothing functions to improve the accuracy of the solutions is an issue that must be investigated further in the near future. Add to that, all the calibration schemes have the possibility of converging to a local optimum. Utilizing probabilistic techniques such as simulated annealing (SA) (Kirkpatrick, Gelatt & Vecchi 1983) to assure that we are converging to a global optimum has the problem of decreasing the speed of convergence. Providing extra constraints for the mentioned calibration schemes which can guarantee the convergence to the real solutions could be one of the challenging areas of research in the future. Moreover, we have shown that the solver noise criterion could be used for revealing the level of accuracy in the calibrated solutions. Investigating possible systematic effects on the solver noise as well as the level of their influence is amongst the main issues for the future work.

ACKNOWLEDGMENTS

REFERENCES

Akaike H., 1973, in Petrov P. N., Lyaki F., eds, Proc. 2nd Second International Symposium on Information Theory. Akademiai Kiado, Budapest, p. 267
Bates D. M., Watts D. G., 2007, Nonlinear Regression Analysis and Its Applications. John Wiley & Sons, New York
Bilmes J., 1998, U. C. Berkely, TR-97-02
Boonstra A., van der Veen A., 2003, IEEE Trans. Signal Processing, 51, 25
Born M., Wolf E., 1999, Principles of Optics. Cambridge Univ. Press, Cambridge
Condon J. J., 1974, ApJ, 188, 279
Feder M., Weinstein E., 1988, IEEE Trans. Acoustics, Speech Signal Processing, 36, 477
Fessler J. A., Hero A. O., 1994, IEEE Trans. Signal Processing, 42, 2664
Gallant A. R., 1975, American Statistician, 29, 73
Graves S., 1978, British J. Philos. Sci., 29, 1
Hamaker J. P., Bregman J. D., Sault R. J., 1996, A&AS, 117, 137
Kirkpatrick S., Gelatt C. D. J., Vecchi M. P., 1983, Sci, 220, 671
Kullback S., 1997, Information Theory and Statistics. John Wiley and Sons, New York
Lampton M., 1997, Comput. Phys., 11, 110
Leshem A., van der Veen A.-J., 2000, IEEE Trans. Information Theory, 46, 1730
Levenberg K., 1944, Q. Appl. Math., 2, 164
Marquardt D. W., 1963, J. Soc. Industrial Appl. Math., 11, 431
Pearson T. J., Readhead A. C. S., 1984, ARA&A, 22, 97
Thompson A. R., Moran J. M., Swenson G. W., 2001, Interferometry and Synthesis in Radio Astronomy, 2nd edn., John Wiley & Sons, New York
van der Tol S., Jeffs B., van der Veen A.-J., 2007, IEEE Trans. Signal Processing, 55, 4497
Wijnholds S., 2010, PhD thesis, TU Delft
Yatawatta S., Zaroubi S., de Bruyn G., Koopmans L., Noordam J., 2009, IEEE 13th Digital Signal Processing Workshop and 5th IEEE Signal Processing Education Workshop, p. 150. IEEE, Piscataway

APPENDIX A: THE EM AND THE SAGE ALGORITHMS

A1 EM algorithm

Considering the complete data $x = [x_1^T \ x_2^T \ldots x_K^T]^T$, where x_is are defined as (8), its PDF will be equal to

$$f_X(x;\theta) = \frac{1}{\pi^{(KM)}|\Sigma|}\exp\{-(x - s(\theta))^H \Sigma^{-1}(x - s(\theta))\}. \quad (A1)$$

In (A1) we have

$$s(\theta) = \left[s_1(\theta_1)^T \ s_2(\theta_2)^T \ \ldots \ s_K(\theta_K)^T \right]^T, \quad (A2)$$

and

$$\Sigma = \begin{bmatrix} \beta_1 \Pi & 0 & \ldots & 0 \\ 0 & \beta_2 \Pi & \ldots & 0 \\ \vdots & \vdots & \ddots & \vdots \\ 0 & 0 & \ldots & \beta_K \Pi \end{bmatrix}. \quad (A3)$$

Therefore, the log-likelihood of the complete data x is derived from

$$\log f_X(x;\theta) = c - \{(x - s(\theta))^H \Sigma^{-1}(x - s(\theta))\}, \quad (A4)$$

where

$$c = -\log\{\pi^{(KM)}|\Sigma|\}.$$

Substituting (A2) and (A3) in (A4), we can rewrite (A4) as

$$\log f_X(\boldsymbol{x};\boldsymbol{\theta}) = c - \sum_{i=1}^{K}\left\{(\boldsymbol{x}_i - \boldsymbol{s}_i(\boldsymbol{\theta}_i))^{\mathrm{H}}(\beta_i\boldsymbol{\Pi})^{-1}(\boldsymbol{x}_i - \boldsymbol{s}_i(\boldsymbol{\theta}_i))\right\}.$$
(A5)

Moreover, the complete data $\boldsymbol{x}$ and the observed data $\boldsymbol{y}$ are related by the below linear transformation

$$\boldsymbol{y} = [\mathsf{I}\ \mathsf{I}\ \dots\ \mathsf{I}]\boldsymbol{x} = \mathbf{G}\boldsymbol{x},$$
(A6)

where $\mathbf{G}$ is a block matrix consisting of the identity matrix I for K times. Thus, they are jointly Gaussian and for a parameter value $\boldsymbol{\theta}'$ we have

$$\widehat{\boldsymbol{x}} = \mathrm{E}\{\boldsymbol{x}|\boldsymbol{y};\boldsymbol{\theta}'\} = \boldsymbol{s}(\boldsymbol{\theta}') + \boldsymbol{\Sigma}\mathbf{G}^{\mathrm{H}}[\mathbf{G}\boldsymbol{\Sigma}\mathbf{G}^{\mathrm{H}}]^{-1}[\boldsymbol{y} - \mathbf{G}\boldsymbol{s}(\boldsymbol{\theta}')].$$
(A7)

Equation (A7) gives us

$$\widehat{\boldsymbol{x}}_i = \boldsymbol{s}_i(\boldsymbol{\theta}_i') + \beta_i\left[\boldsymbol{y} - \sum_{l=1}^{K}\boldsymbol{s}_l(\boldsymbol{\theta}_l')\right]$$
(A8)

as the ith element of the vector $\widehat{\boldsymbol{x}}$.

In applying the EM algorithm, at $(k + 1)$th iteration we would like to find the parameter vector $\boldsymbol{\theta}^{k+1}$ such that maximizes $\mathrm{E}\{\log f_X(\boldsymbol{x};\boldsymbol{\theta})|Y = \boldsymbol{y};\boldsymbol{\theta}^k\}$, where $\boldsymbol{\theta}^k$ is the estimation of $\boldsymbol{\theta}$ obtained at kth iteration. According to (A5) it is exactly equivalent to find $\boldsymbol{\theta}_i^{k+1}$ for each $i \in \{1, 2, \dots, K\}$ such that minimizes $\mathrm{E}\{(\boldsymbol{x}_i - \boldsymbol{s}_i(\boldsymbol{\theta}_i))^{\mathrm{H}}(\beta_i\boldsymbol{\Pi})^{-1}(\boldsymbol{x}_i - \boldsymbol{s}_i(\boldsymbol{\theta}_i))|Y = \boldsymbol{y};\boldsymbol{\theta}^k\}$. Therefore, at the $(k + 1)$th iteration of the algorithm we have:

E Step: calculate

$$\widehat{\boldsymbol{x}}_i^k = \boldsymbol{s}_i\left(\boldsymbol{\theta}_i^k\right) + \beta_i\left[\boldsymbol{y} - \sum_{l=1}^{K}\boldsymbol{s}_l\left(\boldsymbol{\theta}_l^k\right)\right].$$
(A9)

M Step: compute

$$\boldsymbol{\theta}_i^{k+1} = \underset{\boldsymbol{\theta}_i}{\arg\min}\left\|\left[\widehat{\boldsymbol{x}}_i^k - \boldsymbol{s}_i(\boldsymbol{\theta}_i)\right](\beta_i\boldsymbol{\Pi})^{-1/2}\right\|^2,$$
(A10)

for $i \in \{1, 2, \dots, K\}$.

A2 SAGE algorithm

Since in the SAGE algorithm the complete data $\boldsymbol{x}_{W_i}$ is defined as (21), we have

$$\log f_{X_{W_i}}(\boldsymbol{x}_{W_i};\boldsymbol{\theta}_{W_i}) = -\log\{\pi^M|\boldsymbol{\Pi}|\}$$
$$-\left\{\left(\boldsymbol{x}_{W_i} - \sum_{l\in W_i}\boldsymbol{s}_l(\boldsymbol{\theta}_{W_i})\right)^{\mathrm{H}}\boldsymbol{\Pi}^{-1}\left(\boldsymbol{x}_{W_i} - \sum_{l\in W_i}\boldsymbol{s}_l(\boldsymbol{\theta}_{W_i})\right)\right\}.$$
(A11)

At $(k + 1)$th iteration of the algorithm we should calculate the parameter vector $\boldsymbol{\theta}_{W_i}^{k+1}$ which is maximizing $\mathrm{E}\{\log f_{X_{W_i}}(\boldsymbol{x}_{W_i};\boldsymbol{\theta}_{W_i})|Y = \boldsymbol{y};\boldsymbol{\theta}^k\}$. Having (A11), $\boldsymbol{\theta}_{W_i}^{k+1}$ can be derived by minimizing $\mathrm{E}\{(\boldsymbol{x}_{W_i} - \sum_{l\in W_i}\boldsymbol{s}_l(\boldsymbol{\theta}_{W_i}))^{\mathrm{H}}\boldsymbol{\Pi}^{-1}(\boldsymbol{x}_{W_i} - \sum_{l\in W_i}\boldsymbol{s}_l(\boldsymbol{\theta}_{W_i}))|Y = \boldsymbol{y};\boldsymbol{\theta}^k\}$ with respect to $\boldsymbol{\theta}_{W_i}$. Therefore, the SAGE algorithm's steps at the $(k + 1)$th iteration would be written as follows.

SAGE E Step: calculate

$$\widehat{\boldsymbol{x}}_{W_i}^k = \mathrm{E}\left\{\boldsymbol{x}_{W_i}|\boldsymbol{y},\boldsymbol{\theta}^k\right\} = \boldsymbol{y} - \sum_{\substack{j=1\\j\neq i}}^{m}\sum_{l\in W_j}\boldsymbol{s}_l\left(\boldsymbol{\theta}_{W_j}^k\right),$$
(A12)

which is derived from (23).

SAGE M Step: compute

$$\boldsymbol{\theta}_{W_i}^{k+1} = \underset{\boldsymbol{\theta}_{W_i}}{\arg\min}\left\|\left[\widehat{\boldsymbol{x}}_{W_i}^k - \sum_{l\in W_i}\boldsymbol{s}_l(\boldsymbol{\theta}_{W_i})\right](\boldsymbol{\Pi})^{-1/2}\right\|^2,$$
(A13)

for $i \in \{1, 2, \dots, K\}$.

The EM and in particular the SAGE algorithms have the well-known advantage that they ensure that the likelihood gets increased at each iteration step. However, they suffer from two negative features. Their rate of convergence is exponential, and they cannot guarantee the convergence to a global optimum. Nevertheless, they are significantly benefited from choosing a suitable starting point which can be the topic of the future work.

This paper has been typeset from a TEX/LATEX file prepared by the author.